Combustion and Flame 207 (2019) 120–133

Contents lists available at ScienceDirect

Combustion and Flame

journal homepage: www.elsevier.com/locate/combustflame

Prediction of flammable range for pure fuels and mixtures using detailed kinetics

Andrea Bertolino[a,b,c], Alessandro Stagni[c,*], Alberto Cuoci[c], Tiziano Faravelli[c], Alessandro Parente[a,b], Alessio Frassoldati[c]

[a] Aero-Thermo-Mechanics Laboratory, Université Libre de Bruxelles, Ecole polytechnique de Bruxelles, Bruxelles, Belgium
[b] Combustion and Robust Optimization Group (BURN), Université Libre de Bruxelles and Vrije Universiteit Brussel, Bruxelles, Belgium
[c] Department of Chemistry, Materials, and Chemical Engineering "G. Natta", Politecnico di Milano, Milano 20133, Italy

ARTICLE INFO

Article history:
Received 24 November 2018
Revised 2 January 2019
Accepted 20 May 2019

Keywords:
Flammability limits
Chemical kinetics
Soot
Radiation
Laminar flame speed

ABSTRACT

In this work, the flammable range of several hydrocarbons was predicted using a freely-propagating flame method for pure hydrocarbons and their mixtures, investigating the effects of operating conditions, in terms of temperature, pressure, fuel/oxidizer composition. The model showed accurate agreement with a wide set of experimental data. The average deviation between the experiments and the model was reduced to ~20% for the UFL of methanol, methane, ethane, propane, n-butane, n-heptane, ethylene, benzene and two different mixtures, methane/ethylene and methanol/benzene. Model performance was improved for the upper flammability limit by including the effect of soot radiation, modeled using an optically-thin approximation. A comprehensive kinetic mechanism was adopted, and a skeletal kinetic mechanism including a soot sectional model was used to predict soot formation in rich flames. Comparison with Calculated Adiabatic Flame Temperature (CAFT) and Le Chatelier models was also carried out, discussing the advantages of a model including the effects of chemical kinetics. Sensitivity analysis was performed to point out the major role of chemical kinetics especially at the UFL, where chemistry drives the process. This methodology showed that the chemical interaction between two different fuels at the rich limit is the reason for the deviation from the thermally controlled behavior. Finally, chemistry was found to be relevant even for the lean flammability limits predictions of lower alkanes, when pure N_2O is used as oxidizer.

© 2019 The Author(s). Published by Elsevier Inc. on behalf of The Combustion Institute.
This is an open access article under the CC BY license. (http://creativecommons.org/licenses/by/4.0/)

1. Introduction

Chemicals flammability is a topic of the uttermost importance in fire safety engineering. In this context, legislators have always been oriented on risk protection, prescribing the adoption of a number of expensive measures, such as sprinkler system for flame extinction, high structures fire resistance degree, escape route systems, and internal/external hydrant networks; in this field, research towards more innovative techniques for fire suppression is also very active [1]. When it comes to industrial scale incidents [2,3], such actions are often inefficient, since typically industrial plants release a large amount of flammable gas, which is dispersed in the surroundings or inside the building leading to explosions, jet fires, fire balls, flash fires or pool fires if a source of ignition is available. Preventing these phenomena is necessarily associated to the capability of anticipating the occurrence of such events, which implies their understanding at a fundamental level.

Therefore, an accurate prediction of the flammability limits is needed, as they are used for properly estimating the volume of flammable gases. In this regard, Gaussian and Integral models for dispersion modeling have been widely employed, and approaches based on Computational Fluid Dynamics (CFD) to model dispersed flows are becoming more and more common [4], as they show a higher degree of accuracy despite their elevated computational costs.

Coward and Jones [5] published a first extensive data collection on flammability limits, where they were defined as "a borderline composition: a slight change in one direction produces a flammable mixture, in the other direction a non-flammable mixture". The existence of a lower and an upper flammability limit (LFL and UFL, respectively) is intrinsically embedded into this definition: the former occurs in fuel-lean mixtures while the latter in fuel-rich. Zabetakis [6] extended the previous work: both [5] and [6] stress the dependence of the flammability limits on physical

* Corresponding author.
E-mail address: alessandro.stagni@polimi.it (A. Stagni).

https://doi.org/10.1016/j.combustflame.2019.05.036
0010-2180/© 2019 The Author(s). Published by Elsevier Inc. on behalf of The Combustion Institute. This is an open access article under the CC BY license. (http://creativecommons.org/licenses/by/4.0/)

Nomenclature

Roman symbols

b_i	fitting coefficient for Le Chatelier Law [–];
C_p	Constant pressure specific heat [J/(kg . K)]
f_v	soot volumetric fraction [–]
p_k	partial pressure of the kth species participating to radiation [Pa];
Q_{rad}	radiated power [W/m^3];
S_L	laminar flame speed [cm/s];
T	temperature [K];
x	spatial coordinate [m];
y	mole fraction [–];

Greek symbols

α	emissivity [1/m/bar]
δ	soot emissivity [1/m]
σ	Stefan–Boltzmann constant = 5.670e−8 W/m^2/K^4
φ	equivalence ratio [–]
ω	mass fraction [–]

Acronyms

ASTM	American Society for Testing Materials
CAFT	Calculated Adiabatic Flame Temperature
CFD	Computational Fluid Dynamics
FPF	Freely-Propagating Flame
LFL	Lower Flammability Limit [v/v%]
LOC	Limiting Oxygen Concentration [v/v%]
LFS	Laminar Flame Speed [cm s^{-1}]
OTM	Optically Thin Model
PSDF	Particle Size Distribution Function
SA	Sensitivity Analysis
SNB	Statistical Narrow Band
UFL	Upper Flammability Limit [v/v%]
LBS	Limiting Burning Speed [cm s^{-1}]

Subscripts

env	environment
f	flame
i	ith compound inside the fuel/ith pure fuel
j	jth chemical species
k	kth species participating to radiation
L	laminar
LB	limiting burning
ox	oxidiser
mix	mixture-related
rad	radiation

parameters as well as those related to the experimental apparatus. Recent works emphasized the importance of this topic, too. Takahashi et al. [7] tested the flammability of methane and propane using reactors of different shapes, and established their minimum dimensions so as to obtain open-space propagation. Several works discussed the effect of ignition energy on the measurements, and the difference between ignitability and flammability limits [5,6,8]. Wierzba and Wang [9] noticed the wall catalytic effect of capturing H_2 before testing and found out that quartz walls are preferable to steel ones. The first data on flammability limits were obtained using a constant pressure, 1.5 m long vertical tube with bottom ignition and no ceiling [5,6]. ASTM [10,11] proposed a standardized procedure to measure flammability limits in a closed, spherical, and remotely controlled vessel, fitted with pressure and temperature transducers. The latter experimental setup has been widely used in literature [12–14]. The review by Britton [15] attributed a major reliability to this apparatus and discussed the applicability of different criteria to experimentally determine the flammable range. The effect of the vessel volume and shape [7], possible catalytic effect of the walls [9], the choice of the detecting criterion [15], and the accuracy of the measurement tools for temperature, pressure and composition constitute the sources of uncertainty related to the experiments, which has been rarely quantified.

In general, increasing temperature and pressure corresponds to broadening the flammable range [5,6,16–20]. Chen et al. [20] observed the influence of pressure on the increase of buoyancy and the resulting anticipated extinction. The same phenomenon was observed while determining flame speeds in a spherical reactor near flammability limits [21], where they found this effect to be negligible for pressures higher than 5 atm. The influence of oxygen content on the flammable range was also extensively studied: as known, increasing its amount broadens the range [5,6,22,13,23], whereas its depletion leads to a reduction of the difference between UFL and LFL, up to the limiting oxygen concentration (LOC), where they coincide. Changing the oxidizer from air to pure O_2, or nitrous oxide (N_2O), can influence the limits to a significant extent [8,23], and the presence of steam [24] or CO_2 [25] within the oxidizer was shown to suppress flammable limits. Finally, Law et al. [26] showed the effect of flame stretch on flammability limits.

In this scenario, a comprehensive and validated theoretical approach for predicting the flammable ranges of pure fuels and their mixtures would be of the utmost importance within the fire safety community. A formal and theoretical definition of flammability limit was provided by Williams [27], which involves the failure of the propagation of the ideal one-dimensional, steady, laminar, planar, adiabatic flame. Lakshmisha et al. [28,29] stated the importance of the inclusion of a radiative term for modeling heat losses.

Egolfopoulos et al. [30] proposed a "chain-thermal" theory, based on the definition from Williams [27] and the assumption that the competition between branching and termination reactions drives the combustion process nearby the flammability limits, where the flame front propagation slows down, and the heat losses become important [31]. They cause flame temperature to decrease downstream the reaction zone, modifying the reaction pathways and reducing the reaction rates.

A Freely-Propagating Flame (FPF) model with detailed kinetics was adopted to investigate the LFL of methane and propane, and an optically-thin gas radiation model was introduced in order to couple heat losses and kinetics. Van den Schoor et al. [32] extended the work of Egolfopoulos et al. [30] to the UFL of methane at different initial conditions, and compared the performance of several existing kinetic mechanisms. Also, Van den Schoor et al. [33] discussed the approximations intrinsically adopted using the FPF method and applied it to the prediction of the flammability limits of hydrogen/methane/air mixtures. Recently, this method was also used to evaluate the effect of ultra-low temperature on natural gas flammability limits [34].

In this work, the method proposed in [28–30,33] is first extended to include the effect of soot radiation, and then applied to reproduce several data from different experimental configurations, for both pure fuels and mixtures. This paper discusses the applicability of FPF model for the estimation of flammability limits, where the definition of flammability limits is based on the prediction of flame extinction due to radiation heat losses. The radiation effect related to the presence of soot on the predictions of UFL is considered: this is particularly important for aromatic compounds, often constituting a significant fraction of transportation fuel blends [35,36], and at higher pressures [37]. The experimental data from Chang et al. [13,14] are used to demonstrate the flexibility of the method with a wide set of operating conditions, varying initial temperature, pressure and oxidizer compositions for methanol, benzene, and their mixtures.

To the authors knowledge, this is the first time that the "chain-thermal" theory is applied to evaluate the flammability limits of

fuel mixtures containing aromatics and alcohols, and including a soot formation model. Non-negligible differences in the governing chemical paths in stoichiometric and limit conditions are discussed using sensitivity analyses. The accuracy of the method in qualitatively and quantitatively predicting the effect of different oxidizers (i.e. air, pure O_2 and N_2O) on the flammability limits for different fuels is also assessed. Eventually, results are compared with the state-of-the-art approaches to estimate such limits, i.e. the Calculated Adiabatic Flame Temperature (CAFT) method, Le Chatelier law and the use of a Limiting Burning Speed (LBS). The major strengths of the FPF method are thus highlighted. To the purpose, several pure hydrocarbons and their mixtures were investigated.

The remainder of the work is organized as follows. Section 2 describes in detail the state-of-the-art models, highlighting their difference and underlying assumptions, and frames the proposed methodology. Section 3 describes in detail the results obtained through the proposed methodology, for both pure fuels and mixtures at different initial conditions in terms of fuel and oxidizer composition, temperature and pressure. Finally, conclusions are drawn in Section 4.

2. Methodology

2.1. State-of-the-art models

The Calculated Adiabatic Flame Temperature (CAFT) method is widely adopted for computing flammability limits of pure fuels in air and diluted conditions [38–41], and mixtures [22]. Mashuga and Crowl [22] also proposed to consider graphite as a species to be taken into account when calculating UFL. The method embodies the thermal theory on flammability limits proposed by White [42]: a mixture of given composition with assigned initial conditions can be considered as flammable when it is able to reach the limiting burning temperature (T_{LB}), i.e. the temperature where combustion enthalpy and heat losses equate. The method relies on the hypothesis of thermally controlled behavior, which is acceptable for lean mixtures but not for UFL, where chemistry effects become more important [40] and the role of soot formation cannot be disregarded due to its contribution to radiation heat losses. As a matter of fact, a method exclusively based on thermodynamics does not capture the complex process of particulate formation, which grows in rich flames and requires a kinetic knowledge for a proper prediction of the phenomenon [43]. This is one of the reasons why it is not always possible to use a single limiting burning temperature to estimate both LFL and UFL for the same fuel. A $T_{LB} = 1200$ K was proposed in [22], whereas Vidal et al. [40] selected $T_{LB} = 1600$ K to predict LFL of different fuels. Due to such limitation, when mixtures are considered, the use of the same temperature for different fuels may lead to large errors in predictions. The alternative to CAFT for mixtures is the computationally-inexpensive, weighted-average correlation by Le Chatelier, which has been proved to be a particular case of CAFT [44] the following equation:

$$LFL_{mix} = \left[\sum_{i=0}^{n} \frac{y_i}{LFL_i} \right]^{-1} \tag{1}$$

The approximations behind such rule are not always valid for UFL, where the correlation between the known flammability limit values of different fuels, and their standard combustion enthalpy is not linear [45]. Furthermore, Zhao et al. [46] highlighted that the application of Le Chatelier weighted average to methane/ethylene and methane/acetylene binary mixtures leads to large errors in UFL predictions, because of peculiar trends in the limit concentration with respect to the fuel composition. Similar trends were shown by Chang et al. [13,14] for methanol/benzene mixture.

In this work, the CAFT method was applied by minimizing the Gibbs free energy and calculating the Adiabatic Flame Temperature for a given mixture composition and initial conditions.

2.2. Freely-propagating flame model

According to Takahashi et al. [7] and Britton [15], the most accurate experimental procedures for the estimation of the flammable range involves testing flammable mixtures in a spherical bomb. This procedure was frequently used in the past [13,14,22]. Although laminar flame speed measurements have been obtained experimentally in a variety of systems [47–49], nowadays spherical bombs are widely used also for this purpose [50]. This shows the affinity between flammability limits and laminar flame speed, as they are measured in comparable systems. As a consequence, the FPF model can be considered suitable for flammable range estimations, as already discussed [33]. As highlighted by Ranzi et al. [48], the laminar flame speed (S_L) is a fundamental property of a mixture, which entails its diffusivity, exothermicity and reactivity as well as its initial thermodynamic state. It is usually evaluated by assuming a 1-dimensional system, modeled as an adiabatic freely propagating flame. Thus, once the operating conditions and the composition of the mixture are assigned, S_L is determined as the eigenvalue of a system of transport equations [51]. In this study, a radiative term ($\dot{Q}_{rad}$) was considered in the energy conservation equation to account for the flame heat losses. It was modeled through the adoption of an optically thin gas approximation [52,53], which is formalized in the following equation:

$$\dot{Q}_{rad} = 4\sigma \left[\sum_{k=1}^{N_s} p_k \, \alpha_k + \, \delta \right] \left(T^4 - \, T_{env}^4 \right) \tag{2}$$

where σ is the Stefan–Boltzmann constant, p_k and α_k the partial pressure and the Planck mean absorption coefficient for the kth species, respectively, and δ is soot emissivity. The radiative properties of gases are based on the RADCAL model by Grosshandler [54]. The applicability of such a model to improve flame speed calculation was demonstrated in [55,56], where an optically-thin gas model (OTM) was compared with a statistical narrow band model (SNB) for a large set of fuel/air mixtures. This includes the effect of radiation-absorption from reactants, and results in a much higher computational weight. Also, in [33], the OTM was adopted because of its much lower computing demand. However, it is important to notice that for diluted conditions in CO_2 or H_2O, relevant for oxy-fuel and MILD combustion [57], the adoption of the SNB model is necessary in order to correctly predict laminar flame speed [58]. In this work, since the predictions of the UFL require the simulation of a rich flame, a soot emissivity model was included, according to the equation below:

$$\delta = \, C \, f_v \, T \tag{3}$$

where T is the temperature, f_v is the soot volumetric fraction, and C is a fitting constant whose value ($C = 2370$ [1/m/K]) was previously estimated by Widmann [59] by applying a least-square fit on experimental data available in literature in the temperature range between 573 K and 1573 K. Such formulation for soot emissivity was defined by Felske and Tien [60], who used the Milne–Eddington absorption coefficient approximation to derive such formulation. Even though the experimental validation of Eq. (3) is limited, its usage for flammable range estimation is feasible, since this term becomes relevant only for rich cases, which are close to extinction, where the flame temperatures for the analyzed cases respect this range. The kinetic model for particulate formation, which was added to the kinetic mechanisms used in this study is the skeletal version [61] of the one proposed the soot sectional model by Saggese et al. [43]. In this work, this model was further

tested against the data by Mashuga and Crowl [22], who observed soot formation in rich conditions in ethylene premixed flames using a spherical bomb. Supplemental material shows further validation in more detail.

The FPF model describes a laminar flame, which is steady, non-adiabatic, 1-dimensional and planar, and adds several details to the flame description with respect to the CAFT model, resulting in a more accurate description of the phenomena involved in flame propagation. However, FPF model implies some approximations of the complex behavior of the 3D flame propagation occurring inside the spherical bomb, as already discussed in [33]: local flame instabilities, the effect of the flame stretch, and buoyancy are neglected. Spherical coordinates would be needed for modeling the transient stretched flame propagation. This would increase the complexity of the system resulting in a higher computational cost. Also, a 2-dimensional system would be required to model the buoyancy effect [20]. However, Van den Schoor et al. [32] showed that adopting a spherical geometry does not impact significantly on the prediction accuracy. Thus, a mono-dimensional model was adopted in this work. When radiation is considered, the flame temperature decreases, and so do the reaction rates, reducing the overall reactivity. Thus, the characteristic time of the reactive process, which is inversely proportional to S_L, increases. For this reason, in relatively slow flames, like those corresponding to flammability limits, the diffusion phenomena become more important than convection, leading to an increase of the flame thickness. This can be seen in Fig. 2 by comparing the stoichiometric temperature profile with those in LFL and UFL conditions. Therefore, a sufficiently large domain is needed, and in this work it was set to a length of 6.5 cm (this was verified a priori to be large enough for all the cases investigated). For the simulations shown, 50 initial grid points were used, whereas convergence criteria on gradient and curvature coefficients were set to 0.05 and 0.5, respectively. Grid independency was preliminarily verified in test flames, where sensitivity to each of the three parameters was checked. Also, it can be observed that radiation decreases the temperature after the flame front. This effect is more pronounced for the upper limit flame, due to the presence of soot in significant amounts, which is instead negligibly produced in lean mixtures. Figure 1(b) shows the ratio between radiation heat losses and heat released during combustion: close to the upper flammability limits, heat losses are controlled by soot radiation, while only the gas phase radiation is relevant for lean mixtures where soot is not formed.

The study was carried out using the OpenSMOKE++ framework [63,64]. A comprehensive kinetic model from the CRECK Modeling group at Politecnico di Milano [65] was used to describe the chemistry of the fuels investigated in this work, as well as their mixtures. The accuracy in predicting the calculation of S_L for a large number of fuels and fuel mixtures and different operating conditions had been previously demonstrated [48]. The kinetic model is available in CHEMKIN format [66] as supplemental material of this paper, and includes a skeletal version [67] of the soot sectional model by Saggese et al. [43]. The complete mechanism was reduced to a skeletal level through the methodology described in [61,68,67]. A preliminary validation of the flame speed with respect to experimental data was first performed. To the purpose, the large collection of experimental data previously collected [48] was leveraged. Figure 1 shows one example of validation for the laminar flame speed of benzene using the experimental data from Davis and Law [69]. Further validation is reported in the supplemental material. The experimental trend is captured by the model with satisfactory accuracy. It also highlights the effect of equivalence ratio on S_L and temperature, as the mixture approaches limit compositions they show decreasing trend, up to extinction. Right before extinction, S_L is equal to ~4 cm/s when radiation is considered. Experimental values with such low velocities are very scarce

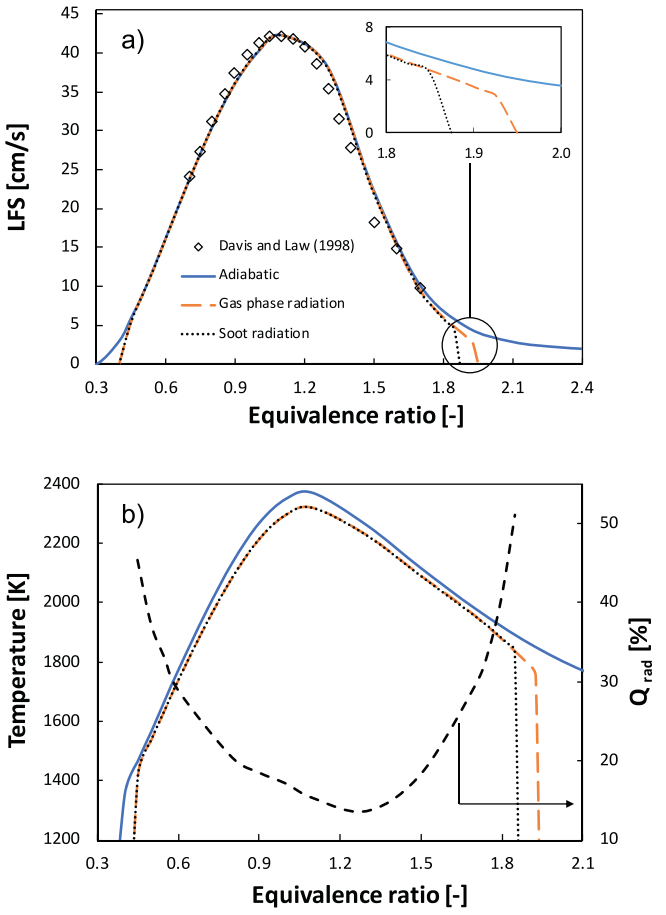

Fig. 1. a) Benzene laminar flame speed as a function of the equivalence ratio, Experimental data from Davis and Law [62]. b) Maximum Temperature and Qrad (—), the percentage of heat losses for radiation considering the soot contribute over the enthalpy of combustion.

in literature, but previous modeling work [70] showed that FPF approach proved effective in such conditions, too.

For the adiabatic case, the flame extinguishes when it reaches an equivalence ratio of ~8.0, leading to a large overestimation at the UFL for Benzene, namely from 6.3%v to 18.3% v/v. On the contrary, adding radiation heat losses due to gas and soot enables the identification of extinction conditions [33,71], coherently with the definition by Williams [27]. The flammability limits were estimated without using any threshold temperature or limiting burning velocity. The mixture composition, corresponding to the last burning flame before the sudden drop of both S_L, and T defines both LFL and UFL. In order to detect the drop in S_L, and T, corresponding to extinction, several values of equivalence ratio were initially simulated. This process was iteratively repeated increasing the number of simulated equivalence ratios between the last burning mixture and the first non-ignitable one. The iteration stopped once a precision of at least 0.1 and 0.05, in terms of equivalence ratio, was reached for UFL and LFL, respectively. This procedure mimics what is usually also performed experimentally [37,72].

Eventually, when the last burning mixture is detected for the case with radiation, sensitivity analysis allows to identify the most relevant kinetic steps. The local normalized sensitivity coefficient s_i is an index of the influence which the ith reaction has on laminar flame speed. It is defined as in (7), where ρS_L is the mass flux and A_i the frequency factor, the s_i:

$$s_i = \frac{A_i}{\rho S_L}\frac{\partial(\rho S_L)}{\partial A_i} \tag{7}$$

Table 1
Summary of considered experiments within this work.

Initial conditions				
Fuel [–]	T [K]	P [bar]	Oxidizer [%]	Reference [–]
CH_3OH	373–473	1–2	11–21% O_2	[13,14]
C_6H_6	373–473	1–2	11–21% O_2	[13,14]
$CH_3OH + C_6H_6$	373–473	1–2	11–21% O_2	[13,14]
CH_4	300	1	Air, N_2O and O_2	[23]
C_2H_6	300	1	Air, N_2O and O_2	[23]
C_3H_8	300	1	Air, N_2O and O_2	[23]
nC_4H_{10}	300	1	Air, N_2O and O_2	[23]
nC_7H_{16}	300	1	Air and O_2	[23]

3. Results and discussion

Table 1 summarizes the cases investigated in this work. The flammability limits of pure methanol and benzene are first investigated in Sections 3.1 and 3.2, respectively. Then, benzene/methanol mixtures are introduced in Section 3.3, and finally the effect of oxidizer and diluent composition is discussed in Sections 3.4 and 3.5, respectively. The overall set of collected experimental data and simulation results is also given in form of tables in the supplementary material.

3.1. Methanol

The validation of the laminar flame speed for methanol is displayed in Fig. 3(a), where good agreement was found between experiments and model predictions. Figure 3(b) shows the dependence of the flammable range on temperature, where both FPF and CAFT methods can accurately predict LFL. However, in terms of upper limit, CAFT significantly underestimates the experimental data, whereas FPF shows a higher accuracy in predicting the absolute values and especially the trend.

Figure 4 highlights methanol flammable range dependence on O_2 concentration in the oxidizer. When O_2 concentration in the oxidizer decreases, the flammable range is significantly reduced. The effect is more pronounced for the UFL limit, since oxygen is the limiting reactant in rich conditions, while it is present in large amounts closer to LFL. The CAFT approach is able to predict the effect of different amounts of oxygen in the oxidizer, but the strong increase of the UFL is underestimated. CAFT would require a threshold temperature higher than 1200 K at low oxygen concentrations and lower than 1200 K at higher oxygen concentrations. On the contrary, the prediction is overall significantly improved using the FPF method. As discussed by Markus et al. [72], a large experimental uncertainty for the determination of UFL is present, mostly because such value is very sensitive to the limit criterion chosen to detect flammability. In Fig. 4, the comparison between two different sets of experimental data from Chang et al. [13,14,76] shows the range of uncertainty in different experimental campaigns.

Figure 5 describes the effect of pressure on the flammable range of methanol. While both models capture the lower limit accurately, the CAFT fails in predicting the UFL increase, as the upper limit increases with increasing pressure. As a matter of fact, pressure does not affect the adiabatic flame temperature calculations to a significant extent, if compared with initial temperature and composition. In the case of FPF, a more accurate prediction is observed, although a deviation is observed at 2 atm. The reason behind it can be traced back to the internal pressure of the reactor during deflagration. Chang et al. [13] measured a maximum internal pressure during deflagration of 3.5 and 18 atm, for 1 and 2 atm operative pressure, respectively. High pressures broaden the flammable range by increasing the experimental upper limit. Since FPF provides steady state solutions for constant pressure, it cannot take into account for a pressure increase induced by the closed volume of the reactor. For this reason, the model underestimates the upper limit at higher pressures. This can also explain the underestimation of UFL at $T = 473$ K (Fig. 3). The large pressure peaks are due to the enhanced reactivity of methanol at high temperatures.

At stoichiometric conditions, Ranzi et al. [48] explained the higher reactivity of methanol with respect to other alcohols by noticing that the hydrogen abstraction reactions on methanol form H_2O_2 and CH_2OH, which easily converts to CH_2O through (R1), without significant formation of the CH_3 radical. Indeed, CH_3 would slow down the fuel reactivity as it reacts with H radicals, terminating the branching chain. Formaldehyde formation justifies the central role of the formyl radical in producing carbon monoxide through reactions (R2), (R3), and (R4). Finally, CO_2 is produced in (R5), which represents a relevant exothermic portion of the combustion process for hydrocarbons [77].

$$CH_2OH(+M) \leftrightharpoons H + CH_2O\ (+M) \quad \text{(R1)}$$

$$HCO(+M) \leftrightharpoons CO + H(+M) \quad \text{(R2)}$$

$$HCO + OH \leftrightharpoons H_2O + CO \quad \text{(R3)}$$

$$HCO + H \leftrightharpoons H_2 + CO \quad \text{(R4)}$$

$$CO + OH \leftrightharpoons CO_2 + H \quad \text{(R5)}$$

Figure 6 shows the sensitivity analysis performed at UFL conditions. H_2O_2 is the main source of hydroxyl radicals through reactions (R6) and (R7), and is formed in large amounts because of the reaction of HO_2 with methanol. The most relevant termination reaction is (R8).

$$H_2O_2\ (+M) \leftrightharpoons 2\ OH(+M) \quad \text{(R6)}$$

$$H_2O_2 + H \leftrightharpoons H_2O + OH \quad \text{(R7)}$$

$$H_2O_2 + O_2 \leftrightharpoons 2\ HO_2 \quad \text{(R8)}$$

At UFL, flame propagation is slower, and formaldehyde is mostly produced through the reaction of hydroxymethyl radical with O_2 in (R9):

$$CH_2OH + O_2 \leftrightharpoons HO_2 + CH_2O \quad \text{(R9)}$$

$$HO_2 + CH_2O \rightarrow H_2O_2 + HCO \quad \text{(R10)}$$

The products of (R9) directly participate to (R10), producing hydrogen peroxide and HCO. The production of HO_2 via (R9) is a key-step, which affects kinetics to a major extent, since for stoichiometric mixtures CH_2OH mostly decomposes through the third body reaction (R1).

The role of HCO changes compared to stoichiometric conditions, replacing CO. In very rich conditions, reaction (R11) tends to extinguish the flame, because of the competing reaction (R12) with HO_2, forming CO_2 and two radicals:

$$HCO\ (+M) \leftrightharpoons CO + H(+M) \quad \text{(R11)}$$

$$HCO + HO_2 \rightarrow CO_2 + H + OH \quad \text{(R12)}$$

The effect of soot-related radiation on the UFL of methanol is negligible since it does not produce particulate in significant amounts.

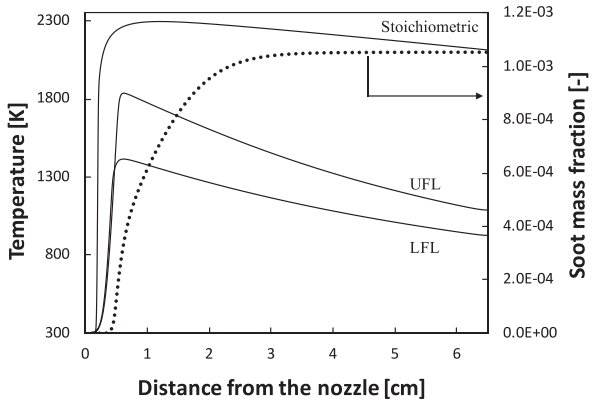

Fig. 2. Temperature profiles of the stoichiometric, lower and upper limit mixtures of a benzene 1D laminar planar flame. The soot mass fraction (•••) was calculated in correspondence of the upper limit mixture.

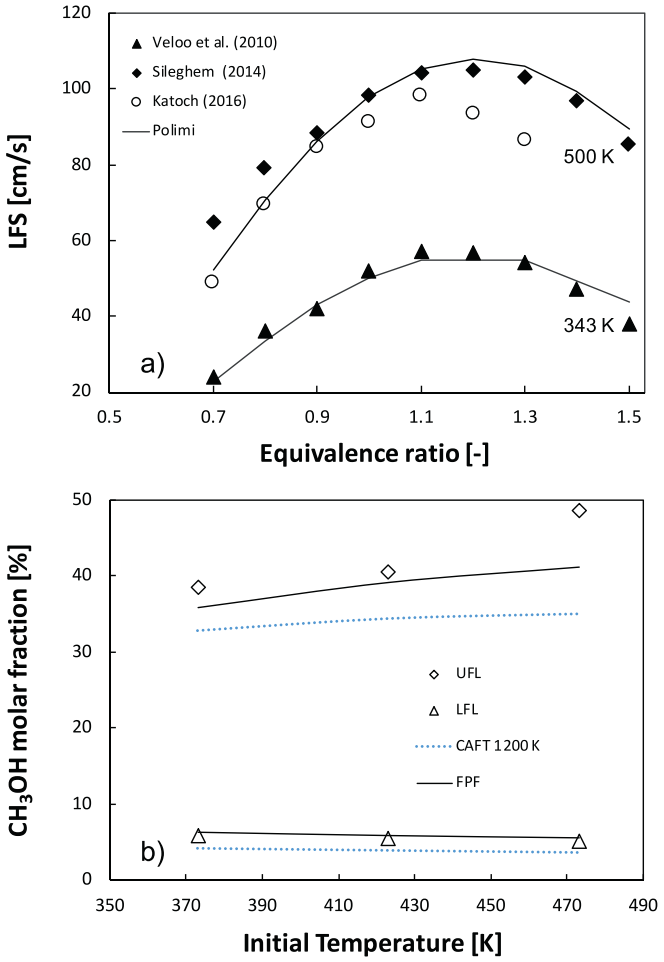

Fig. 3. (a) Methanol flame speed validation. Experimental data from Veloo et al. [73], Katoch [74], and Sileghem [75]. (b) Methanol flammable range dependence from temperature in air at atmospheric pressure. Comparison between FPF and CAFT. Experimental data from Chang et al. [13,14].

3.2. Benzene

The capability of the kinetic mechanism to reproduce the laminar flame speed of benzene was presented in Fig. 2. Further validation is given inside the supplementary material.

Figure 7 shows the prediction of benzene flammable range as a function of temperature. The CAFT method well predicts LFL

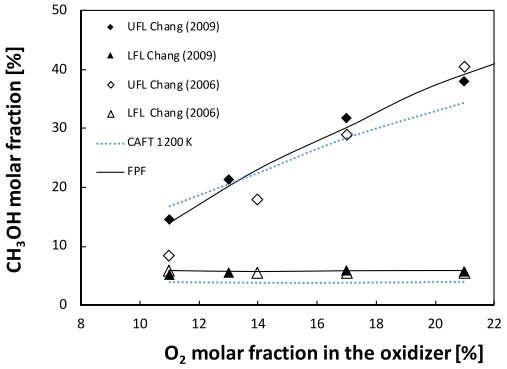

Fig. 4. Methanol flammable range as a function of oxygen percentage concentration in the oxidizer in air at atmospheric pressure and temperature of 423 K. Comparison between FPF and CAFT. Experimental data from Chang et al. [13,14,76].

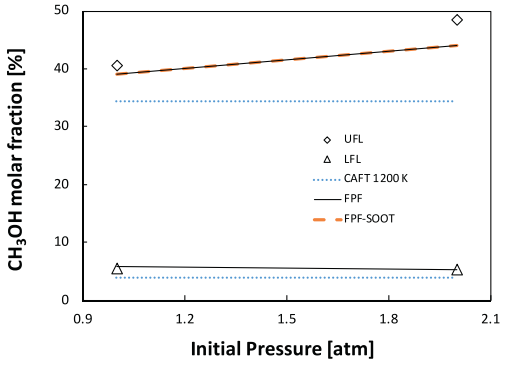

Fig. 5. Methanol flammable range as a function of pressure, at 423 K, in air. Comparison between FPF with, and without (–) soot radiation, and CAFT. Experimental data from Chang et al. [13,14].

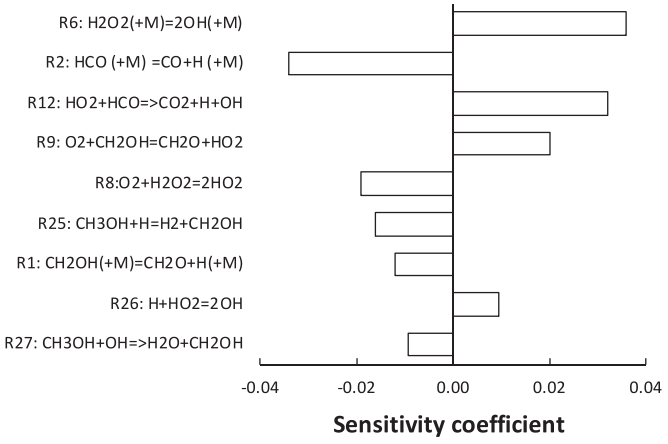

Fig. 6. Methanol sensitivity coefficients on laminar flame speed at UFL conditions, $\varphi = 4.6$, $T = 423$ K and $P = 1$ atm.

and largely overestimates UFL, when the $T_{LB} = 1200$ K criterion is adopted. Better predictions were obtained with $T_{LB} = 1500$ K. On the other side, both FPF methodology and the use of an LBS of 4 cm/s proved accurate for both lower and upper limits.

Figure 8 shows the dependence of the flammable range on the O_2/N_2 ratio within the oxidiser. The CAFT approach with T_{LB}=1200 K significantly overestimates UFL, whereas it correctly predicts the LFL even in this case. A better overall agreement with experiments was found using $T_{LB} = 1500$ K. Therefore, a single T_{LB} providing accurate prediction for both fuels could not be found. Conversely, FPF shows a closer agreement in both cases.

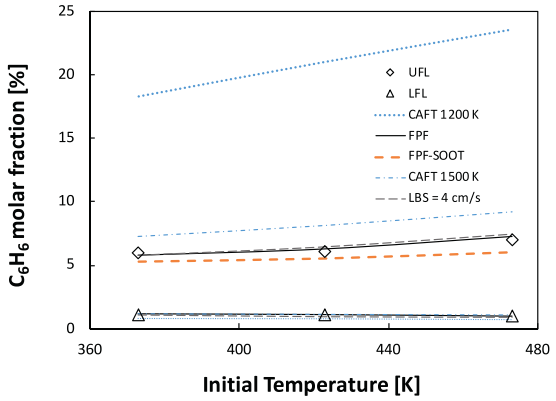

Fig. 7. Benzene flammable range dependence from temperature in air at atmospheric pressure. Comparison between FPF with and without soot radiation, and CAFT. Experimental data from Chang et al. [13,14].

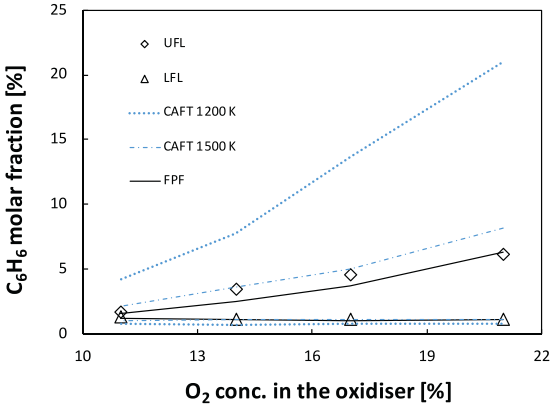

Fig. 8. Benzene flammable range dependence from oxygen percentage concentration in the oxidizer in air at atmospheric pressure and temperature of 423 K. Comparison between FPF and CAFT. Experimental data from Chang et al. [13,14].

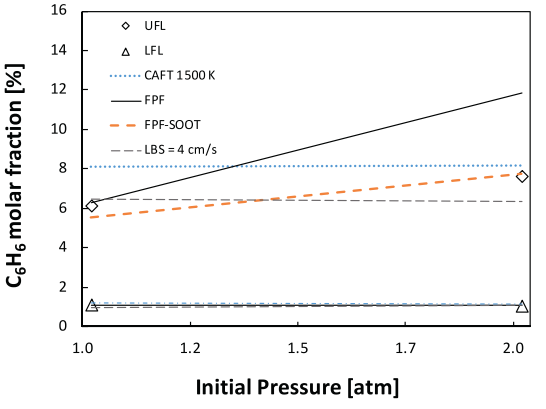

Fig. 9. Benzene flammable range dependence from pressure, in air at 473 K. Comparison between FPF with and without soot radiation, and CAFT. Experimental data from Chang et al. [13,14].

Figure 9 shows the prediction of both LFL and UFL as a function of pressure. As for the case of methanol, the pressure effect is not captured in CAFT method at the UFL, while FPF describes the trend reasonably well. On the other hand, the use of an LBS of 4 cm/s could not predict the variation with pressure. In fact, the laminar flame speed decreases with pressure, thus a constant LBS shifts UFL to leaner mixtures.

When only the radiation term related to gas phase is considered, the model shows a large error for higher pressures. On the contrary, when soot emissivity is included in computing radiation heat losses, predictions are more accurate, and the error at 2 atm decreases from ~56% to ~2%. This occurs because the pressure increase enhances soot formation, on turn increasing the flame emissivity.

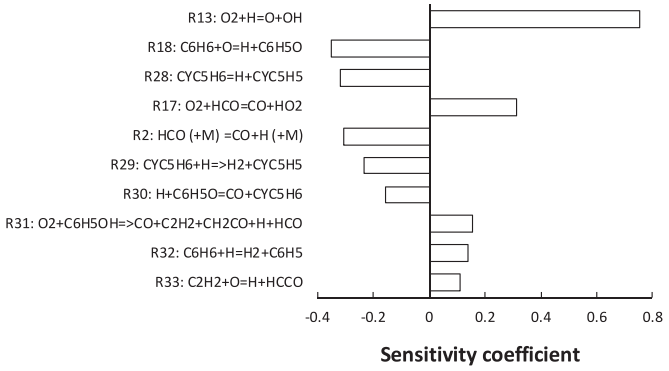

Fig. 10. Benzene sensitivity coefficients on laminar flame speed at UFL conditions, $\varphi = 4.6$, $T = 423$ K and $P = 1$ atm.

The reactivity of a stoichiometric mixture is driven by the competition between reactions (R13) and (R14). Also, the phenoxy radical plays a central role, as deriving from benzene reaction with O radical. C_6H_5O reacts with both H (R15) and O (R16) radicals, leading to the formation of phenol and para-benzoquinone, respectively.

$$H + O_2 \leftrightharpoons OH + O \quad \text{(R13)}$$

$$OH + H(+M) \leftrightharpoons H_2O(+M) \quad \text{(R14)}$$

$$C_6H_5O + H \leftrightharpoons C_6H_5OH \quad \text{(R15)}$$

$$C_6H_5O + O \leftrightharpoons C_6H_4O_2 + H \quad \text{(R16)}$$

Figure 10 shows the sensitivity analysis on laminar flame speed of benzene in proximity of the UFL. The most sensitive reaction is (R13), but as for the case of methanol, (R11) turns to a negative effect on reactivity because of competition with reaction (R17) which does not form H radicals.

The recombination reactions of H radicals with phenoxy radicals strongly reduce the flame reactivity. Moreover, the direct formation of resonantly-stabilized cyclopentadienyl radicals from phenoxy radicals further reduces the system reactivity, because of the recombination with H radicals to form cyclopentadiene. H-abstraction reactions from cyclopentadiene lead to cyclopentadienyl radicals, favoring termination reactions and further consuming the H radicals. For this reason, the formation of HO_2 radicals favors the system reactivity, whereas reaction (R18), which directly produces phenoxy radical, exhibits the largest negative sensitivity coefficient:

$$O_2 + HCO \leftrightharpoons HO_2 + CO \quad \text{(R17)}$$

$$C_6H_6 + O \leftrightharpoons C_6H_5O + H \quad \text{(R18)}$$

3.3. Benzene/methanol mixture

One of the major strengths of the FPF method lies in the capability to predict the effect of pressure on flammable range and the UFLs for fuel mixtures. Zhao et al. [46] experimentally observed deviations from the thermally controlled behavior for different binary mixtures of hydrocarbons at the UFL conditions. Although Mashuga and Crowl [22] successfully predicted the flammability

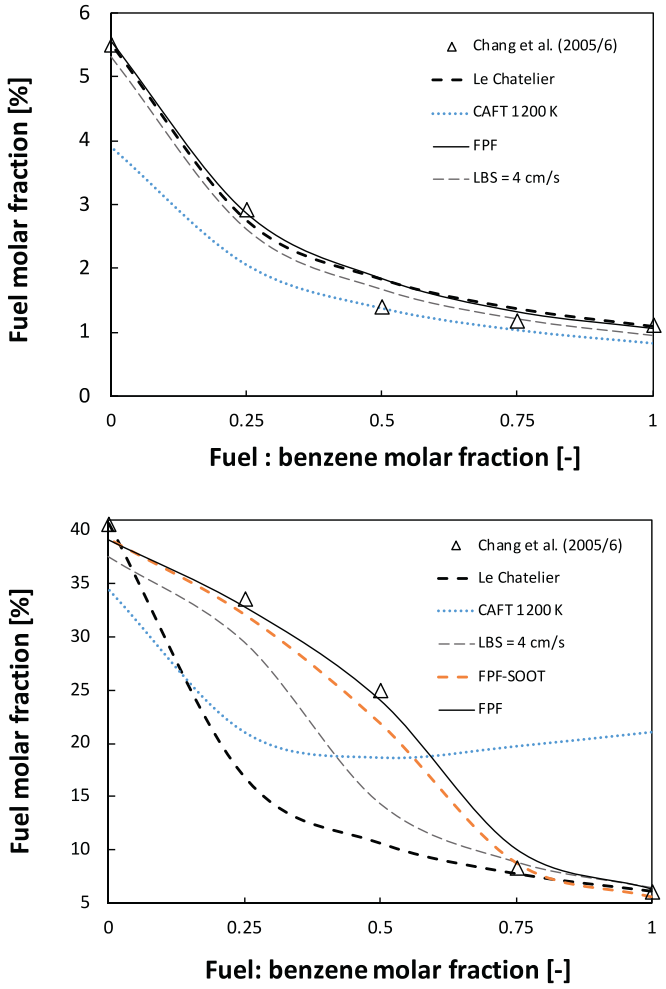

Fig. 11. Flammable range of methanol/benzene mixture as a function of fuel composition at 1 atm, and 423 K, in air. Experimental data from Chang et al. [13,14].

limits for a 50/50 mixture of methane and ethylene using CAFT with a threshold temperature of 1200 K, Zhao et al. [46] showed that the above-mentioned deviations occur for different intermediate fuel compositions. They also pointed out that a single adopted power-law correction on Le Chatelier law, shown in the below equation.

$$LFL_{mix} = \left[\sum_{i=0}^{n} \frac{(y_i)^{b_i}}{LFL_i} \right]^{-1} \tag{8}$$

does not find correspondence with experimental data or mutual correlation when applied to different hydrocarbon binary mixtures [46]. In the equation above, b_i represents a fitting coefficient which is usually derived from experimental measurements. Similarly to the case of Zhao et al. [46], even more pronounced UFL deviations from the thermally controlled behavior were found among the experiments by Chang et al. [13,14] on methanol/benzene mixtures.

Figure 11 shows LFL and UFL of these mixtures. The only method that is able to accurately predict the (kinetics-driven) UFL extinction is FPF. This occurs because Le Chatelier law was derived under the hypothesis of segregation between the pure fuels chemistry, as well as CAFT model. Additionally, for CAFT, a single threshold adiabatic temperature is not applicable to both lower and upper limits since it is not possible to use the same value for both the components. Nevertheless, Le Chatelier law agrees with the data for benzene concentrations equal or greater than 75%. Eventually, also the use of a constant limiting burning speed (4 cm/s) fails to reproduce the interaction between the fuels. Thus, the interaction between the chemistry of the two pure fuels becomes non-negligible for leaner fuel mixtures in benzene. A fundamental explanation of the origin of the observed deviations at the UFL is given below.

Table 2
Detail of the limiting burning temperature for some relevant benzene/methanol cases.

$(y_{C_6H_6})_{fuel}$ [–]	$(y_{O_2})_{ox}$ [–]	$(T_{LB})_{UFL}$ [K]
1	0.11	1582
0.5	0.11	1597
0	0.11	1252
1	0.21	1612
0.5	0.21	1153
0	0.21	1056

Figure 12 displays the sensitivity analysis on flame speed for a 50/50 fuel composition, for $P = 1$ atm, $T = 423$ K and different oxidizer compositions. The most important reaction for flame propagation is (R21), which does not have a relevant impact on sensitivity analysis either on methanol or on benzene pure chemistry. The H abstraction on the pure fuels leads to the formation of phenyl and hydroxymethyl radicals. The competition for oxygen consumption between (R9), (R19), and (R20) reduces the oxidizer availability.

$$C_6H_5 + O_2 \leftrightharpoons C_6H_4O_2 + O \tag{R19}$$

$$C_6H_5 + O_2 \leftrightharpoons C_6\ H_5O + O \tag{R20}$$

$$CH_3\ OH + HO_2 \leftrightharpoons H_2\ O_2 + CH_2\ OH \tag{R21}$$

Therefore, HO_2 offers an alternative path for methanol oxidation in (R21), by directly forming H_2O_2, which is also produced through (R10). Indeed, H_2O_2 plays a key role in the boost of reactivity through (R1), forming two OH radicals. Thus, (R21) and in general the oxidation pathway that proceeds via HO_2 and H_2O_2 represents the overall effect of the chemical interactions between the two fuels, causing the inaccuracy of both CAFT and Le Chatelier approaches. This pathway ($HO_2 \rightarrow H_2O_2 \rightarrow OH$) does not produce large amounts of H radical, which are involved in the chain termination reactions with phenoxy radicals. Figure 13 shows this kinetic path in detail.

Figure 14 shows the effect of changing the oxygen content in the oxidizer. The sensitivity analysis in Fig. 12 shows that the presence of a large concentration of O_2 enhances the role of HO_2((R8), (R17)). In these conditions, the role of the chain branching reaction $H + O_2 = OH + O$ is more limited. On the contrary, the sensitivity analysis at low-oxygen concentration shows a larger sensitivity coefficient for the $H + O_2 = OH + O$ reaction and the HCO decomposition to H and CO. The experiments show that a kinetics-driven trend becomes evident for oxygen mole fractions higher than ~14%. In these conditions, Le Chatelier law is not capable of reproducing the experimental data accurately. Thus, two different trends can be identified, i.e. a thermally controlled regime for O_2 contents lower or equal to 14% and kinetics-driven for the others (17%, 21%, 100%). On the other hand, the FPF method well predicts both the observed regimes because it includes a comprehensive description of the already mentioned competition between kinetic pathways as well as of flame structure, i.e. reaction, diffusion, convection and radiation. Table 2 reports the values of the limiting burning temperatures for the 11% and 21% oxygen cases calculated with FPF model, for the pure fuels and the 50/50 mixtures.

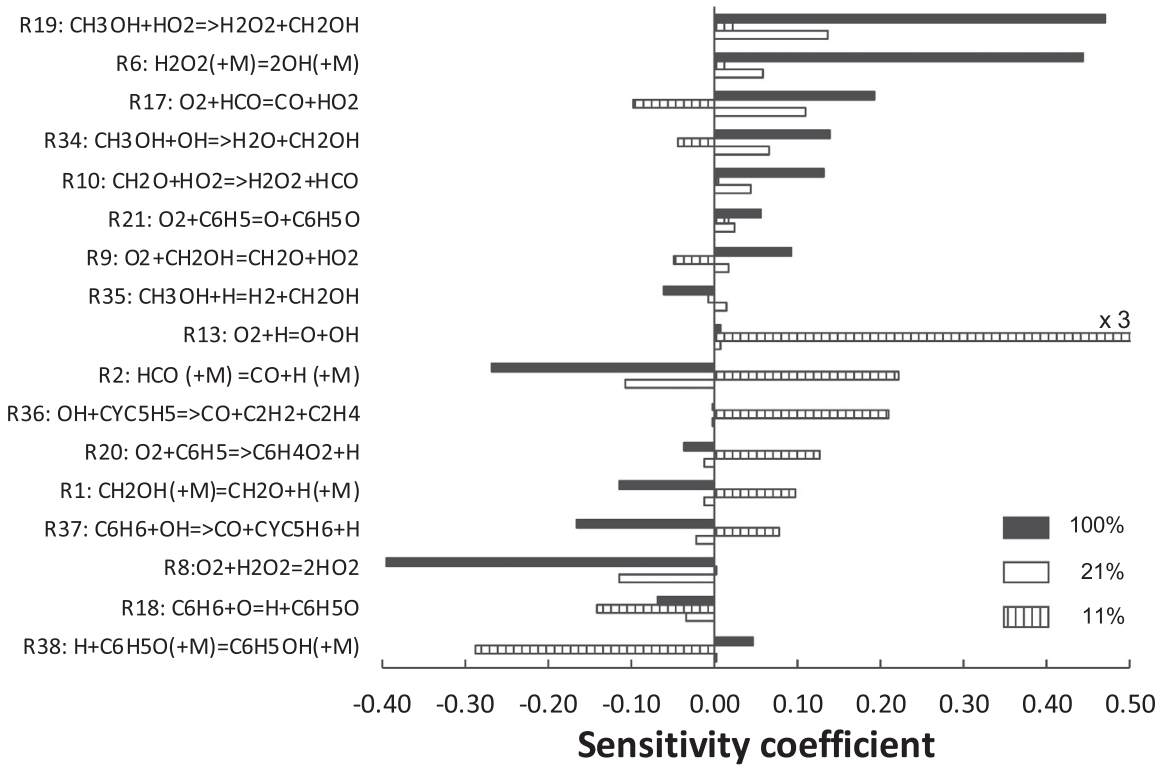

Fig. 12. Sensitivity analysis for 50/50 benzene/methanol mixtures dependence with different oxygen percentage concentration in the oxidizer, namely 11, 21, 100%, atmospheric pressure and 423 K.

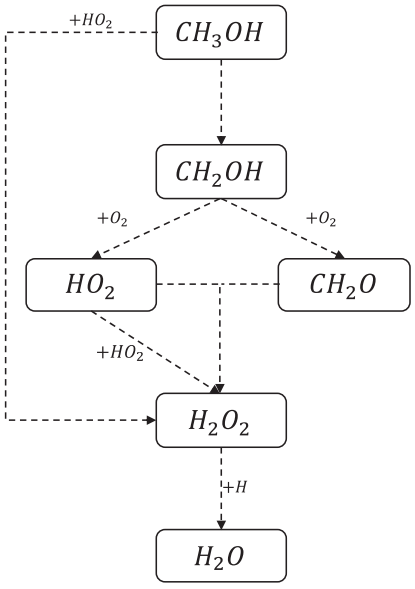

Fig. 13. Flux analysis for 50/50 mixtures, oxygen percentage concentration in the oxidizer 21% at 1 atm and 423 K.

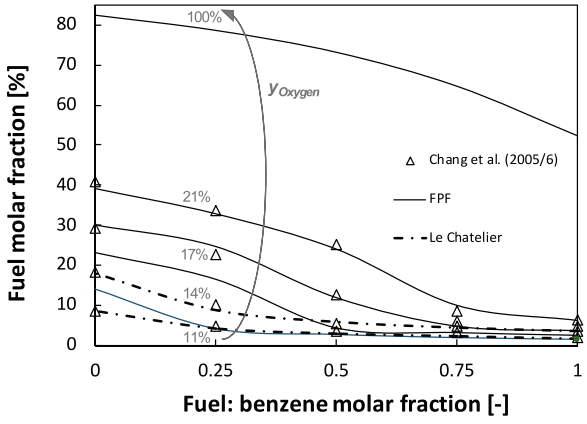

Fig. 14. Methanol/Benzene mixture upper flammability limit dependence from oxygen percentage concentration in the oxidizer, at 1 atm, and 423 K. Experimental data from Chang et al. [13,14].

When O_2 concentration is closer to LOC, the mixture extinguishes for temperature values similar to those of benzene. In fact, even though the oxygen content is lower, UFL corresponds to an equivalence ratio of ∼1.13, where the flame is more reactive, showing a limiting burning speed of ∼6.8 cm/s in the simulations. Under these conditions, benzene and methanol are oxidized almost simultaneously, reaching complete conversion. Furthermore, the hydroxymethyl radical decomposition occurs through between (R4) and (R9), such that benzene can react with oxygen in spite of being slower. In the case where oxidizer is air, the higher oxygen content causes the fuel to extinguish for higher equivalence ratios, namely ∼6.8, where the flame speed is much lower (∼1.6 cm/s). In this case, the temperature of the last burning mixture is comparable to the one of pure methanol. This explains the S-shaped UFL, which tends to be similar to that of pure alcohol for higher benzene fractions, as the O_2 content increases. The role of HO_2 reaction with alcohols in supporting the reactivity in diluted conditions was already investigated by different authors [78–81].

The flame structure analysis revealed the faster conversion of CH_3OH: it reacts more quickly with hydroxyl radical in the first part of the flame. Within this zone, benzene reactivity is much slower, and this results in its negligible oxidation. Downstream, C_6H_5 reacts with oxygen through (R20). Due to this competition,

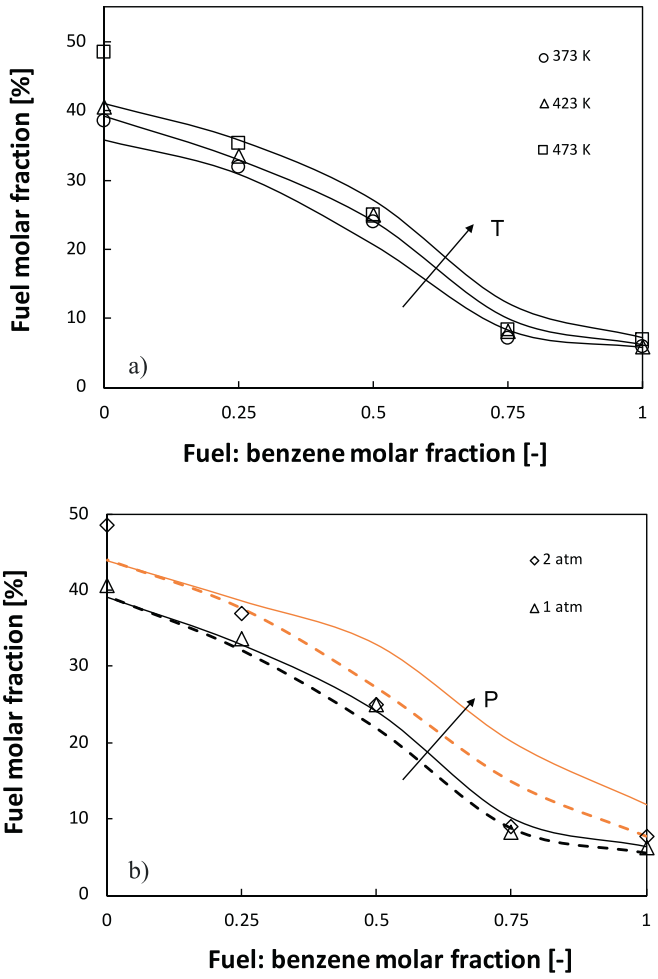

Fig. 15. (a) Upper flammability limit of methanol/benzene mixture as a function of temperature. (b) Upper flammability limit of methanol/benzene mixture as a function of pressure at 423 K, in air. Comparison between FPF model with (- - -) and without (–) soot radiation. Experimental data from Chang et al. [13,14].

methanol decomposes mainly through (R21), reacting with HO_2 in turn, and enhances the reactivity through H_2O_2, as previously mentioned. This explains the deviations from the thermally controlled behaviour observed. Therefore, chemistry is the origin of the differences among the LOC case and the others. This is evident in Fig. 12, too: benzene chemistry is dominant for low oxygen contents, while it becomes less important for air and pure oxygen. The chemical interaction between the two fuels becomes even stronger for oxy-combustion, where the typical Le Chatelier trend is reversed (see Fig. 14).

Figure 15 shows the dependence of UFL on temperature and pressure. Both effects are reproduced with reasonable accuracy by the FPF model. The effect of temperature on UFL is quite important for methanol rich mixtures, while it is less important for pure benzene. The model is able to predict this trend, although the effect for pure methanol is underestimated especially for $T = 473$ K. The main difference is the very large fuel concentration at UFL for methanol compared to benzene. Using the same scale, the effect of temperature on the concentration of benzene at the UFL might look negligible, but an increase of about 15% moving from 373 K to 473 K is actually present in the experiments, and is well predicted by the model. It is also worth noting how the consideration of soot emissivity impacts on the UFL estimation for both $P = 1$ atm (Fig. 11) and 2 atm pressure values (Fig. 15). As previously explained, the influence of soot is stronger for higher pressures. Moreover, in both cases the radiative term begins to influence the flammability limits for molar fractions of benzene, within the fuel, larger than ~0.25.

3.4. Effect of oxidizer composition

Figure 16 shows the results of Koshiba et al. [23] on the flammability limits of *n*-alkanes with different types of oxidizer. Here only cases with air, pure oxygen, and N_2O as oxidizers are presented. Simulations were carried out on methane, ethane, propane, n-butane and n-heptane. The sub-mechanism for N_2O kinetics was validated in [82]. Figure 16 shows that when oxidizer is air, the flame speed method accurately predicts both the rich and lean limits trends. It is important to point out that data on air were obtained on a lab-scale facility, which is different from the one of Koshiba et al. [23], and more similar to that of Chang et al. [13,14]. On the contrary, data in pure O_2 and N_2O were obtained directly from Koshiba et al. [23]. The gap between the prediction of UFL and the related measurements increases with decreasing the oxygen content in the inlet mixture. This can be attributed to the vessel shape and dimensions, which has a diameter of 10 cm, and a height of 12 cm. Such reactor has a significant surface/volume ratio, such that the quenching effect due to the walls strongly affects the measurement by extinguishing the flame at lower equivalence ratios. The quenching effect becomes more and more important with temperature differences increasing between the flame and the walls, and it is more pronounced in oxy-combustion conditions, where the flame temperature is higher.

Data available from Mashuga and Crowl [22] on methane/pure oxygen combustion are also shown in Fig. 16, and they support this hypothesis, since their estimation is closer to the simulations, and also found consistency with data in [13,14]. Such data were obtained into a 20 l spherical vessel, which meets the Takahashi criteria for unconfined self-propagation [7]. Figure 16 points out that the presence of N_2O increases the upper flammability limits for methane, ethane, propane, and n-butane with respect to the case of air. This is due to the decomposition of nitrous oxide via (R22), such that an oxygen molar fraction of about 33.3% is virtually obtained within the oxidizer, i.e. higher than O_2 concentration in air:

$$N_2O\ (+M) \leftrightharpoons N_2 + 0.5\ O_2\ (+M) \quad \text{(R22)}$$

$$N_2O + O \leftrightharpoons N_2 + O_2 \quad \text{(R23)}$$

$$N_2O + O \leftrightharpoons 2NO \quad \text{(R24)}$$

The reaction (R22) also enhances the fuel reactivity due to its negative combustion enthalpy $\Delta H_c = -82.1$ kJ mol^{-1}, occurring at a temperature higher than 750 K, and participating to the exothermicity of the process, as reported by Koshiba et al. [23]. Flame speed calculations for pure N_2O were performed for several temperatures. At temperatures higher than 750 K, N_2O shows its own flame speed, which is ~4.5 cm/s and reaches a peak temperature of ~1930 K. The sensitivity coefficients for these conditions are reported in Fig. 17. Reactions (R22) and (R23) drive the reactivity, while NO_x formation in 7 tends to lead the flame to extinction.

Oxy-combustion also results in higher UFL values, since in these conditions the limiting factor is the oxygen availability, which allows a large fuel conversion and sustains the flame at lower temperatures. With pure oxygen, T_{LB} of methane is 1600 K and burning velocity is equal to ~4.5 cm/s, while in N_2O T_{LB} =1800 K and the flame speed is approximately ~10 cm/s. This indicates that when the oxidizer is N_2O, its decomposition sustains the flame reactivity (extinction temperature is very close to the one developed by pure N_2O), whereas for pure oxygen combustion the limiting factor

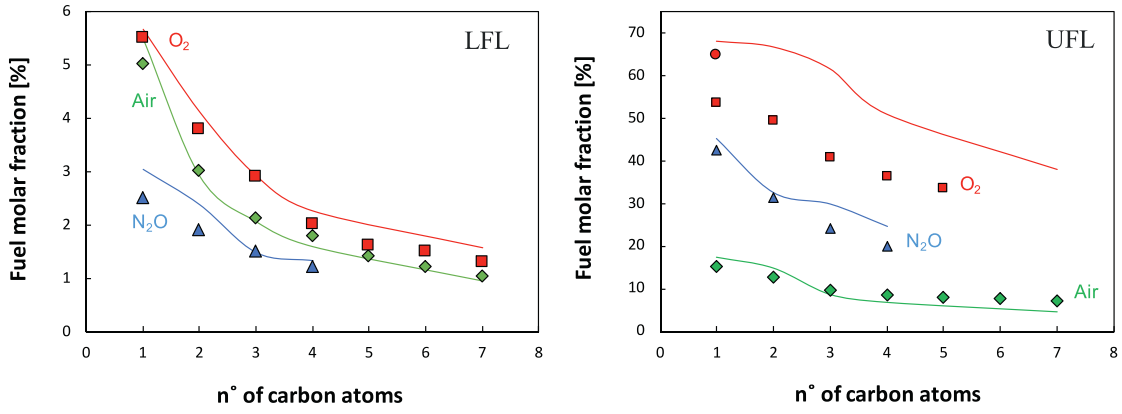

Fig. 16. Dependence of low alkanes flammable ranges on different oxidizer compositions: air (green), N_2O (light-blue) and pure O_2 (red). Experimental data from Koshiba et al. [23] and (○) from Mashuga and Crowl [22]. (For interpretation of the references to colour in this figure legend, the reader is referred to the web version of this article.)

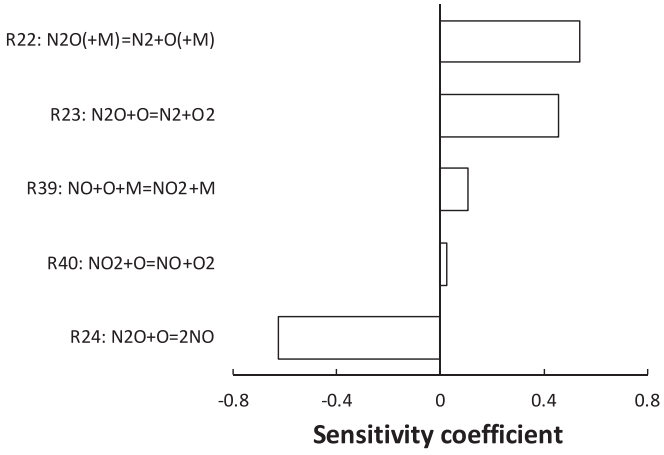

Fig. 17. Sensitivity coefficients for the flame speed of pure N_2O flame at 750 K and 1 atm.

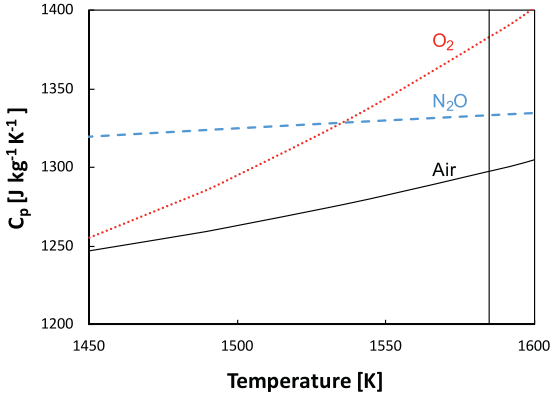

Fig. 18. The constant pressure specific heat dependence from temperature for different oxidizers. The vertical line represents the extinction temperature for methane at the LFL according to FPF calculations.

is the fuel reactivity. An interesting effect is the higher LFLs with pure oxygen with respect to those in air. Close to the lean limit, reactivity is indeed driven by the available amount of fuel and its average specific heat. More importantly, the specific heat of reactants influences the flame temperature by subtracting heat from the reaction zone. Figure 18 shows the differences between the specific heats of the oxidizers, as a function of temperature. For the calculated extinction temperature in oxy-fuel combustion regime, a larger amount of heat is necessary to bring the reactants from the initial temperature to the flame temperature compared to that of air, and nitrogen oxide, due to the larger specific heat of pure O_2. Combustion in both oxygen and air shows a limit flame temperature of ∼1580 K, which explains the unusual LFL behavior for oxy-combustion. As a result, when the oxidizer is N_2O, the specific heat should lie between the previous two, but LFL is even lower compared to that in air. This behavior, too, is due to the exothermic decomposition of nitrous oxide for temperature values higher than 750 K. This additional heat generated makes a larger amount of mixture available for ignition by enhancing flame reactivity near the limits. The sensitivity analysis performed on alkanes up to n-butane confirmed that reaction (R22) is the most important for the four of them (cf. Supplemental material).

The FPF method was applied for the prediction of the flammable ranges for a wider set of fuels and mixtures in order to complete validation. In addition to the cases described before, the method was applied to:

- methane;
- ethane;
- propane;
- n-butane;
- n-heptane;
- ethylene;
- benzene;
- methane/ethylene mixtures with variable relative compositions;

Overall, the average prediction error was lowered from ∼30% to ∼10% for the lean limit and from ∼50% to ∼20% for the rich limit, considering a wide set of operative conditions. The parity plots of Fig. 19 show these results with deeper detail FPF and CAFT. For the sake of clarity, here only one condition per each fuel was displayed, while further details can be found in Tables 1 and 2 in the Supplementary material. As already outlined in the first part of this section, significant improvements in accuracy are observed by using the FPF model. This is even more apparent at the UFL.

3.5. Effect of diluent composition on the flammability limits

LFL and UFL prediction under diluted conditions is a topic of great interest for safety engineering [39,40], as they narrow the flammable range as the dilution rises. Several experiments were performed in CERN by Besnard [83], taking different inert species in account, namely $C_2H_2F_4$, SF_6, CF_4, CO_2, H_2O He, N_2 and Ar, only at atmospheric conditions. Lately, Molnarne et al. [84] used these measurements to develop a predictive method based on the so called “coefficient of nitrogen equivalency”, which they declare not to be applicable for upper limit predictions. They also discussed the chemical reactivity of some of these diluents, such as $C_2H_2F_4$, SF_6, CF_4, and CO_2, which not only increase the average

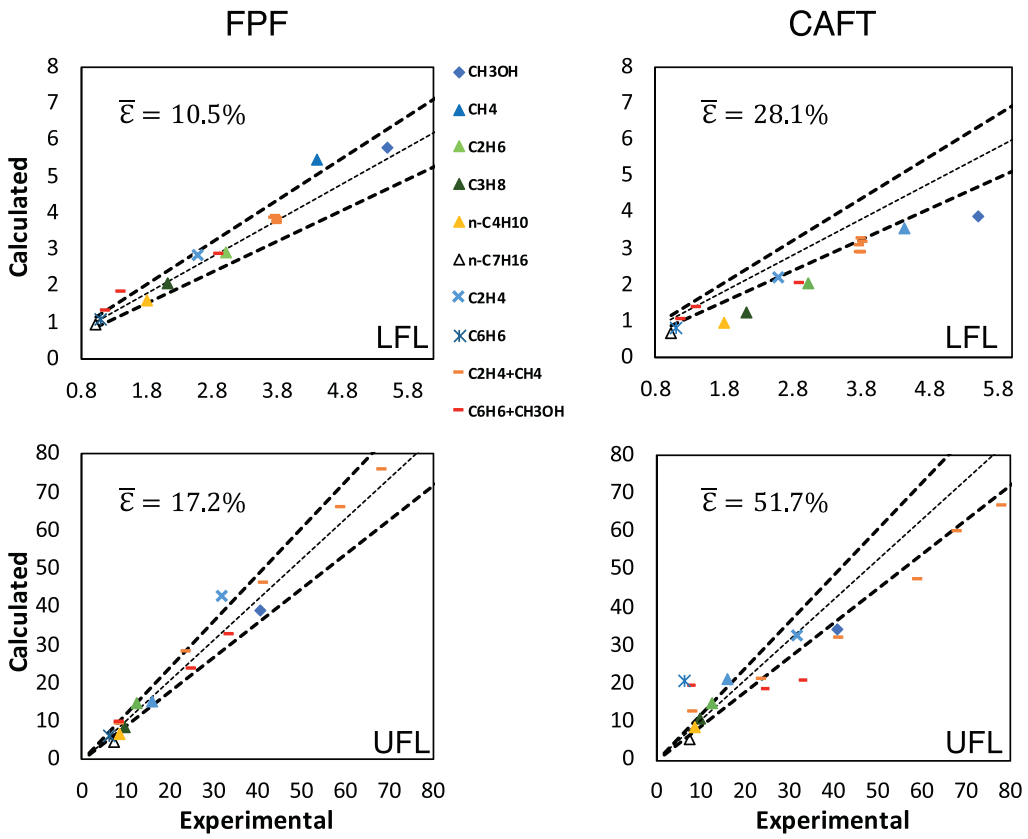

Fig. 19. Scatter plot: experimental vs. calculated lower and upper flammability limits. CAFT estimations were obtained with T_{LB} = 1200 K. The two dashed black lines limit the region where the uncertainty is 15%. Experimental data from [5,6,13,14,22,32,40,46].

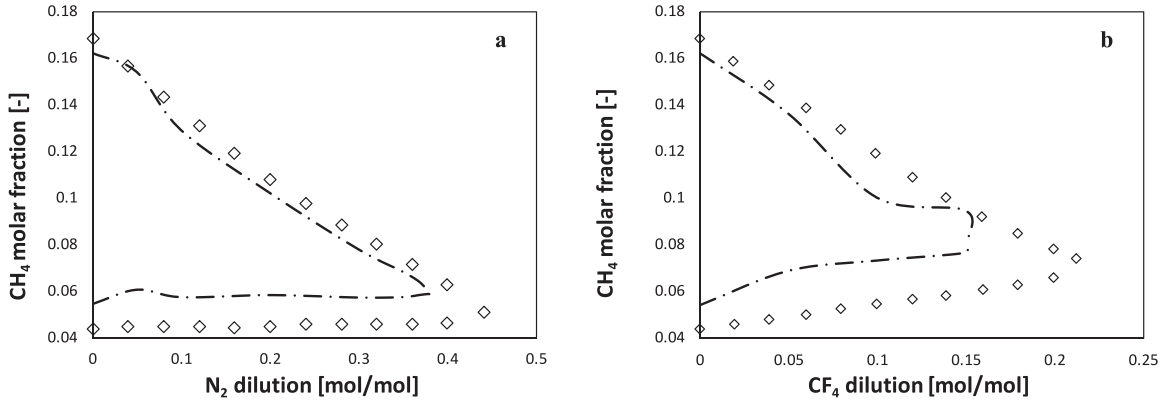

Fig. 20. Methane flammable range as a function of the nitrogen dilution (a) and carbon tetrafluoride (b). Experimental data from Besnard [83].

specific heat of the non-reactive part of the mixture, but also play a role in the fuel chemistry. The applicability of FPF method for N_2 and CF_4 was assessed, using a kinetic mechanism from Saso et al. [85]. Even though Fig. 20 shows that the FPF method underestimates the flammable range, it has to be pointed out that Bernard [83] used the DIN-51649 experimental procedure for measurements. Yet, DIN-51649 was shown to overestimate the flammable range with respect to other methods [15], as the threshold mixtures are considered to be the flammability limits even though they are not able to properly propagate a flame. This definition is usually applied in order to obtain what Zabetakis [6] referred to as ignitability limits. For this reason, since the FPF method defines the flammable limit as a mixture which is able to infinitely propagate a flame front, its predictions can be considered as reasonable. Figure 20 shows that the FPF approach is able to predict the large reduction in the flammability range of methane when CF_4 replaces N_2 as a diluent. Adding 20% of CF_4 is sufficient to suppress methane flammability, whereas the same limit is reached only adding more than 40% of nitrogen.

4. Conclusions

In this work, the Freely Propagating Flame (FPF) approach was applied for the prediction of flammability limits considering the effects of soot on radiation, and the consequent extinction.

The validation of FPF approach against a wide set of experimental data showed its superior accuracy compared the state-of-the-art methodology to predict flammability limits, i.e. Le Chatelier law and CAFT method applied with a single temperature threshold, and LBS method with a threshold of 4 cm/s. Pressure and temper-

ature effects were considered and discussed in detail for methanol, benzene and different mixtures of the two fuels: in particular, for the first time (to the authors knowledge) these fuel mixtures were simulated using FPF. Remarkable results were obtained at the UFLs, especially for pressure dependency, where CAFT and LBS method were proven to be inaccurate. In the case of mixtures, the chemical interaction between two fuels, which was experimentally detected, was explained using sensitivity and flux analysis. Such interaction was shown to weaken with decreasing the oxygen concentration. A proper description of radiation turned out to be an essential element to achieve stronger an accurate prediction capability, especially for rich benzene flames at high pressure, where soot increases the mixture emissivity. Methane, ethane, propane, n-butane, and n-heptane flammability limits were addressed using air, pure oxygen, and nitrous oxide. For the nitrous oxide, other chemical interactions with the fuel were proven. Although the computational effort associated with the FPF approach is larger than CAFT, several advantages in using such a method could be identified:

1. The interaction between detailed chemistry and radiation could be accounted for. As a matter of fact, radiation highly influences the flame propagation because of the low reactivity that characterizes the limit mixtures. The importance of including a soot sub-mechanism and radiation model at UFL was demonstrated. Also, the increasing relevance of soot with pressure has been quantified, as it promotes the formation of solid particulate;
2. A common criterion for detecting flammability limits of different fuels was identified, i.e. the observation of the flame extinction in a freely propagating flame model. On the other side, the general disagreement on a proper and single threshold value for the CAFT and LBS. Compared to traditional CAFT methods with a single threshold (1200 K), the error is reduced by a factor of 3. The unfeasibility of Le Chatelier law for predicting the upper limit could be confirmed;
3. Sensitivity analysis could be carried out throughout FPF methodology, thus shedding light on fuel chemistry at the upper limit, where extinction is kinetically controlled. Specifically, the most important reactions for methanol- and benzene-rich mixtures were identified and compared with the results for the stoichiometric flames previously obtained in [48]. This allowed to detect the chemical interaction between them in the mixtures of the two compounds, for the first time in literature to the authors' knowledge. This also explains why the thermal-based methods are not capable of an accurate estimation of UFL trend with fuel composition, which was already experimentally pointed out by Zhao et al. [46], but without any fundamental explanation.
4. The flammable range can be accurately predicted also in the case of non-conventional oxidizers (e.g., N_2O), which significantly shift both flammability limits, as well as for different diluents and/or flame retardants (e.g., fluorinated compounds).

Further work can be carried out on the extension of FPF model to diluted conditions, investigating wider ranges of initial conditions (in terms of temperature and pressure), different fuel mixtures and oxidizer composition. To this purpose, the radiation model would need proper improvement, since it should account for the presence of CO_2 and H_2O, when present as bath gases. In such cases, a more accurate evaluation of their effect on their emissivity would be needed [86].

Acknowledgments

The first author acknowledges the support of Funds pour la Recherche Scientifique (FNRS) through a FRIA fellowship of the project "HOPTIMAL: Hierarchical development of OPTimised kinetic Mechanisms for Advanced combustion technoLogies". This project has received funding from the European Research Council (ERC) under the European Union's Horizon 2020 research and innovation programme under grant agreement No 714605.

Supplementary materials

Supplementary material associated with this article can be found, in the online version, at doi:10.1016/j.combustflame.2019.05.036.

References

[1] H. Li, X. Chen, C.-M. Shu, Q. Wang, Y. Zhang, Experimental and numerical investigation of the influence of laterally T sprayed water mist on a methane–air jet flame, Chem. Eng. J. 356 (2019) 554–569.
[2] S. Copelli, V. Torretta, D. Massa, C. Sala Cattaneo, M. Derudi, R. Rota, Runaway reactions and vapour cloud explosions: the synthron case study, Chem. Eng. Trans. 36 (2014) 115–120.
[3] L. Marmo, N. Piccinini, L. Fiorentini, The thyssen krupp accident in torino: investigation methods, accident dynamics and lesson learned, Ital. Assoc. Chem. Eng. (AIDIC) 26 (2012) 615–620.
[4] R. Longo, M. Fürst, A. Bellemans, M. Ferrarotti, M. Derudi, A. Parente, CFD dispersion study based on a variable Schmidt formulation for flows around different configurations of ground-mounted buildings, Build. Environ. 154 (2019) 336–347.
[5] H.F. Coward, G.W. Jones, Limits of flammability of gases and vapors, Bureau of Mines, 1952.
[6] M.G. Zabetakis, Flammability characteristics of combustible gases and vapors, Bureau of Mines, 1965.
[7] A. Takahashi, Y. Urano, K. Tokuhashi, S. Kondo, Effect of the vessel size and shape on experimental flammability limits of gases, J. Hazard. Mater. (2003) 27–37.
[8] U.J. Pfahl, M.C. Ross, J.E. Shepherd, Flammability limits, ignition energy, and flame speeds in H_2–CH_4–NH_3–N_2O–O_2–N_2, Combust. Flame (2000) 140–158.
[9] I. Wierzba, Q. Wang, The flammability limits of H_2–CO–CH_4 mixtures in air at elevated temperatures, Int. J. Hydrog. Energy (2006) 485–489.
[10] American society for Testing and Materials, "Standard Practice for Determining Limits of Flammability of Chemicals at Elevated Temperature and Pressure", ASTM E918-83, ASTM, Conshohocken, PA (2007).
[11] ASTM E 681-01, Standard test method for concentration limits of flammability of chemicals (vapors and gases), 2001.
[12] H. Cheikhravat, N. Chaumeix, A. Bentaib, C.-E. Paillard, Flammability limits of hydrogen–air mixtures, Nucl. Technol. 178 (1) (2012) 5–16.
[13] Y.M. Chang, J.M. Tseng, C.M. Shuand, K.H. Hu, Flammability studies of benzene and methanol with various vapour mixing ratios at 150 °C, Korean J. Chem. Eng. (2005) 803–812.
[14] Y.M. Chang, K.H. Hu, J.K. Chen, C.M. Shu, Flammability studies of benzene and methanol with different vapour mixing ratios under various initial conditions, J. Therm. Anal. Calorim. 83 (2006) 107–112.
[15] L.G. Britton, Two hundred years of flammable limits, The Dow Chemical Company, 2002.
[16] H.-J. Liaw, K.-Y. Chen, A model for predicting temperature effect on flammability limits, Fuel (2016) 179–187.
[17] B. Vanderstraeten, D. Tuerlinckx, J. Berghmans, S. Vliegen, E. Van't Oost, B. Smit, Experimental study of the pressure and temperature dependence on the upper flammability limit of methane/air mixtures, J. Hazard. Mater. (1997) 237–246.
[18] S. Kondo, K. Takizawa, A. Takahashi, K. Tokuhashi, On the temperature dependence of flammability limits of gases, J. Hazard. Mater. (2011) 585–590.
[19] G. Cui, C. Yang, Z.-L. Li, Z. Zhou, J.-L. Li, Experimental study and theoretical calculation of flammability limits of methane/air mixture at elevated temperatures and pressures, J. Loss Prevent. Process Ind. (2016) 252–258.
[20] J.-R.- Chen, H.-Y. Tsai, J.-H. Chien, H.-J. Pan, Flow and flame visualization near the upper flammability limits of methane/air and propane/air mixtures at elevated pressures, J. Loss Prevent. Process Ind. 24 (2011) 662–670.
[21] Z. Chen, X. Qin, B. Xu, Y. Ju, F. Liu, Studies of radiation absorption on flame-speed and flammability limit of carbon dioxide diluted methane flames at elevated pressures, Proc. Combust. Inst. 31 (2007) 2693–2700.
[22] C.V. Mashuga, D.A. Crowl, Flammability zone prediction using calculated adiabatic flame temperatures, Process Saf. Progress 18 (1999) 127–134.
[23] Y. Koshiba, T. Nishida, N. Morita, H. Ohtani, Explosion behaviour of n-alkane/nitrous oxide mixtures, Process Saf. Environ. Prot. (2015) 11–15.
[24] M.J. Degges, J.E. Boyer, K.K. Kuo, L. Basini, Influence of steam on the flammability limits of premixed natural gas/oxygen/steam mixtures, Chem. Eng. J. 165 (2010) 633–638.
[25] W. Qin, F.N. Egolfopoulos, T.T. Tsotsis, Fundamental and environmental aspects of landfill gas utilization for power generation, Chem. Eng. J. 82 (1–3) (2001) 157–172 Vols..
[26] C.K. Law, D.L. Zhu, G. Yu, Propagation and extinction of stretched premixed flames, 21st Symposium (International) on Combustion (1986).
[27] F.A. Williams, Combustion Theory, Benjamin/Cummings, Menlo, CA/Reading, MA, 1985.

[28] K.N. Lakshmisha, P.J. Paul, K.S. Rajan, G. Goyal, H.S. Mukunda, Behaviour of methane–oxygen–nitrogen mixtures near flammability limits (1988), pp. 1573–1578.
[29] K. Lakshmisha, P.J. Paul, H.S. Mukunda, On the flammability limit and heat loss in flames with detailed chemistry (1991), pp. 433–440.
[30] F.N. Egolfopoulos, A.T. Holley, C.K. Law, An assessment of the lean flammability limits of CH_4/air and C_3H_8/air mixtures at engine-like conditions, Proc. Combust. Inst. 31 (2007) 3015–3022.
[31] S.D. Brian, L.J. Wilfrid, A theory of inflammability limits and flame-quenching, Proceedings of the Royal Society of London. Ser. A Math. Phys. Eng. Sci. 240 (1220) (1957) 83–100.
[32] F. Van den Schoor, F. Verplaetsen, J. Berghmans, Calculation of the upper flammability limit of methane/air mixtures et elevated pressures and temperatures, J. Hazard. Mater. 153 (2008) 1301–1307.
[33] F. Van den Schoor, R.T. Hermanns, J.A. van Oijen, F. Verplaetsen, L.P. de Goey, Comparison and evaluation of methods for the determination of flammability limits, applied to methane/hydrogen/air mixtures, J. Hazard. Mater. (2008) 573–581.
[34] G. Pio, E. Salzano, The effect of ultra-low temperature on the flammability limits of a methane/air/diluent mixtures, J. Hazard. Mater. 362 (2019) 224–229.
[35] W.J. Pitz, C.J. Mueller, Recent progress in the development of diesel surrogate fuels, Progr. Energy Combust. Sci. 37 (3) (2011) 330–350.
[36] E. Ranzi, A. Frassoldati, A. Stagni, M. Pelucchi, A. Cuoci, T. Faravelli, Reduced kinetic schemes of complex reaction systems: fossil and biomass-derived transportation fuels, Int. J. Chem. Kinet. 46 (9) (2014) 512–542.
[37] M. Goethals, B. Vanderstraeten, J. Berghmans, G. De Smedt, S. Vliegen, E. Van't Oost, Experimental study of the flammability limits of toluene–air mixtures at elevated pressure and temperature, J. Hazard. Mater. 70 (1999) 93–104.
[38] M.R. Brooks, D.A. Crowl, Flammability envelopes for methanol, ethanol, acetonitrile and toluene, J. Loss Prevent. Process Ind. 20 (2007) 144–150.
[39] S.Y. Liao, D.M. Jiang, Z.H. Huang, Q. Cheng, J. Gao, Y. Hu, Approximation of flammability region for natural gas–air–diluent mixture, J. Hazard. Mater. A125 (2005) 23–28.
[40] M. Vidal, W. Wong, W.J. Rogers, M.S. Mannan, Evaluation of lower flammability limits of the fuel-air-diluent mixtures using calculated adiabatic flame temperatures, J. Hazard. Mater. 130 (2006) 21–27.
[41] S.-H. Qin, X.-X. Sun, W.-C. Lin, C.-M. Shu, F. You, S.-C. Ho, Experimental and computational approaches for CH_4 and C_2H_4 flammability zones, Energy Fuels 31 (9) (2017) 9950–9956.
[42] A.G. White, Limits for the propagation of flame in inflammable gas-air mixtures. Part III. The effects of temperature on the limits, J. Chem. Soc. 127 (1925) 672–684.
[43] C. Saggese, S. Ferrario, J. Camacho, A. Cuoci, A. Frassoldati, E. Ranzi, H. Wang, T. Faravelli, Kinetic modeling of particle size distribution of soot in a premixed burner-stabilized stagnation ethylene flame, Combust. Flame 162 (2015) 3356–3369.
[44] C.V. Mashuga, D.A. Crowl, Derivation of Le Chatelier's mixing rule for flammable limits, Process Saf. Progr. 19 (2000).
[45] T. Suzuki, Empirical relationship between lower flammability limits and standard enthalpies of combustion of organic compounds, Fire Mater. (1994) 333–336.
[46] F. Zhao, W.J. Rogers, M.S. Mannan, Experimental measurement and numerical analysis of binary hydrocarbon mixture flammability limits, Process Saf. Environ. Prot. 87 (2009) 94–104.
[47] J. Li, Q. Li, Y. Wang, Z. Guo, X. Liu, Fundamental flame characteristic of premixed H_2-air combustion in a planar porous micro-combustor, Chem. Eng. J. 283 (2016) 1187–1196.
[48] E. Ranzi, A. Frassoldati, R. Grana, A. Cuoci, T. Faravelli, A.P. Kelley, C.K. Law, Hierarchical and comparative kinetic modeling of laminar flame speeds of Hydrocarbon and Oxygenated fuels, Prog. Energy Combust. Sci. 38 (2012) 468–501.
[49] F. Egolfopoulos, N. Hansen, Y. Ju, K. Kohse-Höinghaus, C.K. Law, F. Qi, Advances and challenges in laminar flame experiments and implications for combustion chemistry, Prog. Energy Combust. Sci. 43 (2014) 36–67.
[50] R. Grosseuvres, A. Comandini, A. Bentaib, N. Chaumeix, Combustion properties of $H_2/N_2/O_2$/steam mixtures (2018), pp. 1537–1546.
[51] T. Poinsot, D. Veynante, Theoretical and numerical combustion, Edwards, 2001.
[52] M.F. Modest, Radiative Heat Transfer, McGraw-Hill, New York, 1993.
[53] M. Modest, D.C. Haworth, Radiation effects in laminar flames, Radiative heat transfer in turbulent combustion systems, Springer, 2016 Briefs in applied sciences and technology.
[54] W.L. Grosshandler, RADCAL: a narrow-band model for radiation calculations in a combustion envirnoment, 1993 NIST Technical Note, 1402, NIST.
[55] H. Hu, W. Han, J. Santner, X. Gou, C.H. Sohn, Y. Ju, Z. Chen, Radiation-induced uncertainty in laminar flame speed measured from propagating spherical flames, Combust. Flame 161 (2014) 2815–2824.
[56] H. Nakamura, M. Shindo, Effects of radiation heat loss on laminar premixed ammonia/air flames, Proc. Combust. Inst. (2018) 1741–1748.
[57] M. De Joannon, A. Cavaliere, Mild Combustion, Prog. Energy Combust. Sci. 30 (2004) 329–366.
[58] Z. Chen, Effect of radiation absorption on spherical flame propagation and radiation-induced uncertainty in laminar flame speed measurement, Proc. Combust. Inst. 36 (2017) 1129–1136.
[59] J.F. Widmann, Evaluation of the Planck Mean Absorption coefficients for radiation transport through smoke, Combust. Sci. Technol. 175 (2003) 2038–2299.
[60] J.D. Felske, C.L. Tien, The use of the Milne–Eddington absorption coefficient for radiative heat transfer in combustion system, Trans. ASME J. Heat Transf. (1977) 456–458.
[61] A. Stagni, A. Frassoldati, A. Cuoci, T. Faravelli, E. Ranzi, Skeletal mechanism reduction through species-targeted sensitivity analysis, Combust. Flame 163 (2016) 382–393.
[62] S.G. Davis, C.K. Law, Determination of and fuel structure effects on laminar flame speeds of C1 to C8 hydrocarbons, Combust. Sci. Technol. 140 (1998) 427–449.
[63] A. Cuoci, A. Frassoldati, T. Faravelli, E. Ranzi, Comput. Phys. Commun. 192 (2015) 237–264.
[64] A. Cuoci, A. Frassoldati, T. Faravelli, E. Ranzi, Numerical modeling of laminar flames with detailed kinetics based on the operator-splitting method, Energy Fuels 27 (2013) 7730–7753.
[65] T.C.M. Group, "http://creckmodeling.chem.polimi.it/".
[66] R.J. Kee, F.M. Rupley, J.A. Miller, CHEMKIN: a Fortran chemical kinetics package for the analysis of gas-phase chemical and plasma kinetics, Livermore, CA, 1989 Sandia Report SAND89-8009, Sandia National Laboratory.
[67] A. Stagni, A. Cuoci, A. Frassoldati, E. Ranzi, T. Faravelli, Numerical investigation of soot formation from microgravity droplet combustion using heterogeneous chemistry, Combust. Flame 189 (2018) 393–406.
[68] P. Pepiot-Desjardins, H. Pitsch, An efficient error-propagation-based reduction method for large chemical kinetic mechanisms, Combust. Flame 154 (1–2) (2008) 67–81.
[69] S.G. Davis, C.K. Law, Determination of the fuel structure effects on laminar flame speeds of C1 to C8 hydrocarbons, Combust. Sci. Technol. (2007) 427–449.
[70] H. Nakamura, M. Shindo, Effects of radiation heat loss on laminar premixed ammonia/air flames, Proc. Combust. Inst. (2018) 1741–1748.
[71] L. Qiao, Y. Gan, T. Nishiie, W.J.A. Dahm, E.S. Oran, Extinction of premixed methane/air flames in microgravity by diluents: effects of radiation and Lewis number, Combust. Flame 157 (2010) 1446–1455.
[72] D. Markus, H.-P. Schildberg, W. Wildner, G. Krdzalic, U. Maas, Flammability limits of premixed methane/methanol/air flames, Combust. Sci. Technol. (2003) 2095–2112.
[73] P.S. Veloo, Y.L. Wang, F.N. Egolfopoulos, C.K. Westbrook, A comparative experimental and computational study of methanol, ethanol, and n-butanol flames, Combust. Flame (2010).
[74] Katoch, Measurement of laminar burning velocities of methanol-air mixtures at elevated temperatures, Fuel (2016).
[75] Sileghem, Laminar burning velocities of primary reference fuels and simple alcohols, Fuel (2014).
[76] Y.-M. Chang, J.-C. Lee, C.-C. Chen, C.-M. Shu, Fire and explosion properties examinations of toluene–methanol mixtures approached to the minimum oxygen concentration, J. Therm. Anal. Calorim. (2009) 741–749.
[77] I. Glassman, R.A. Yetter, Combustion, 4th edition, Elsevier, 2008.
[78] M. Bissoli, A. Frassoldati, A. Cuoci, E. Ranzi, T. Faravelli, A model investigation of fuel and operating regime impact on homogeneous charge compression ignition engine performance, Energy Fuels 32 (2018) 2282–2298.
[79] Barraza-Boret, L. Cesar, S.W. Wagnon, Woolridge, S. Margaret, Combustion chemistry of ethanol: ignition and speciation studies in a rapid compression facility, J. Phys. Chem. 120 (2016) 7408–7418.
[80] M. Sjöberg, J. Dec, Effects of EGR and its constituents on HCCI autoignition of ethanol, Proc. Combust. Inst. 33 (2011) 3031–3038.
[81] T.J. Held, F.L. Dryer, A comprehensive mechanism for methanol oxidation, Int. J. Chem. Kinet. 30 (1998) 805–830.
[82] A. Frassoldati, T. Faravelli, E. Ranzi, A wide range modeling study of NO_x formation and nitrogen chemistry in hydrogen combustion, Int. J. Hydrog. Energy (2006) 5170–5183.
[83] M. Molnarne, P. Mizsey, V. Schröder, Flammability of gas mixtures: Part 2: Influence of inert gases, J. Hazard. Mater. 121 (1-3) (2005) 45–49.
[84] M. Molnarne, P. Mizsey, V. Schröder, Flammability of gas mixtures. Part 2: influence of inert gases, J. Hazard. Mater. A121 (2005) 45–49.
[85] Y. Saso, D.L. Zhu, H. Wang, C.K. Law, N. Saito, Laminar burning velocities of trifluoromethane–methane mixtures: experiment and numerical simulation, Combust. Flame 114 (1998) 457–468.
[86] T.F. Smith, Z.F. Shen, J.N. Friedman, Evaluation of coefficients for the weighted sum of gray gases model, J. Heat Transf. 104 (4) (1982) 602–608.